HHS Public Access

Author manuscript

Neuron. Author manuscript; available in PMC 2023 November 16.

Published in final edited form as:

Neuron. 2022 November 16; 110(22): 3820–3832.e4. doi:10.1016/j.neuron.2022.09.011.

Prefrontal-Habenular Microstructural Impairments in Human Cocaine and Heroin Addiction

Sarah G. King[1], **Pierre-Olivier Gaudreault**[1], **Pias Malaker**[1], **Joo-won Kim**[2], **Nelly Alia-Klein**[1], **Junqian Xu**[2,*], **Rita Z. Goldstein**[1,*]

[1]Departments of Psychiatry and Neuroscience, Icahn School of Medicine at Mount Sinai, New York, New York, USA 10029

[2]Departments of Radiology and Psychiatry, Baylor College of Medicine, Houston, Texas, USA 77030

Summary

The habenula (Hb) is central to adaptive reward and aversion-driven behaviors, comprising a hub for higher-order processing networks involving the prefrontal cortex (PFC). Despite an established role in preclinical models of cocaine addiction, the translational significance of the Hb, and its connectivity with the PFC, in humans is unclear. Using diffusion tractography, we detailed PFC structural connectivity with the Hb and two control regions, quantifying tract-specific microstructural features in healthy and cocaine-addicted individuals. White matter was uniquely impaired in PFC-Hb projections in both short-term abstainers and current cocaine users. Abnormalities in this tract further generalized to an independent sample of heroin-addicted individuals and were associated, in an exploratory analysis, with earlier onset of drug use across the addiction subgroups, potentially serving as a predisposing marker amenable for early intervention. Importantly, these findings contextualize a plausible PFC-Hb circuit in the human brain, supporting preclinical evidence for its impairment in cocaine addiction.

eTOC blurb:

The habenula receives direct input from the prefrontal cortex, driving drug-seeking behaviors in preclinical models of addiction. Using diffusion MRI, King et al. identified microstructural abnormalities in the structural connections of the prefrontal cortex and habenula in humans with cocaine or heroin addiction, extending the translational importance of this circuit.

Corresponding Author: Rita Z. Goldstein, rita.goldstein@mssm.edu.
Lead Contact: Rita Z. Goldstein, rita.goldstein@mssm.edu
*equal contribution

Author contributions: S.G.K., N.A-K., J.X., and R.Z.G. conceptualized and designed the research. J.K. and J.X. advised on the methods. S.G.K. performed the data analysis. S.G.K., P-O.G., J.K., J.X., and R.Z.G. interpreted the results. P.M. collected and managed the data. S.G.K. wrote the initial draft of the manuscript. P-O.G., N.A-K., P.M., J.K., J.X., and R.Z.G. revised the manuscript.

Declaration of interest: The authors declare no competing interests.

Keywords

cocaine addiction; heroin addiction; habenula; prefrontal cortex; anterior limb of the internal capsule; diffusion tractography; premorbid markers

Introduction

Impaired reward valuation is a fundamental feature of drug addiction that is characterized by compulsive drug-seeking at the expense of alternative reinforcers (Koob & Volkow, 2016). Dysregulation of the prefrontal cortex (PFC), which is integral to the brain networks that regulate reward processing, salience attribution, and inhibitory control, is proposed to precipitate bingeing and relapse, perpetuating the addiction cycle (Goldstein & Volkow, 2002, 2011). The habenula (Hb), a reward-processing structure in the epithalamus, plays a critical role in connecting regions underlying emotion and cognitive processing, notably the basal ganglia/striatum and amygdala, but also the PFC (Chiba et al., 2001; Kim & Lee, 2012; Zahm & Root, 2017). Within the reward system, the lateral nucleus of the Hb (LHb) conveys aversion-related information to monoamine-releasing nuclei, thereby regulating motivated behaviors and reward sensitivity (Hikosaka, 2010). Specifically, neurons in the LHb trigger aversive responses to undesirable events, signaling to the rostromedial tegmental nucleus to suppress reward-sensitive neurotransmission in the dopaminergic midbrain (Jhou et al., 2009; Matsumoto & Hikosaka, 2009).

The LHb has been increasingly recognized as a key neural substrate of chronic pathological substance use (Pribiag et al., 2021; Velasquez et al., 2014), with emerging preclinical evidence implicating it in drug-seeking and addiction. Specifically, certain LHb neurons show biphasic responses to cocaine, including an initial downregulation (marking a drug-induced “high”) followed by sustained increased firing (Gill et al., 2013; Jhou et al., 2013). Further, excitatory signaling from the rodent PFC to the LHb (Navailles et al., 2015), and the LHb to the rostromedial tegmental nucleus (Mahler & Aston-Jones, 2012), increased when cocaine-seeking behaviors were suppressed in a behavioral model of drug-related inhibition. Lasting LHb activation is consistent with aversive states that define withdrawal and, by promoting stress-induced cocaine-seeking, this mechanism may play a role in mediating the transition from initial use to long-term dependence, craving, and relapse (Meye et al., 2015, 2016). Notably, whereas habenula functional abnormalities have also been detailed in models of opioid and nicotine addiction (Mathis & Kenny, 2019), the role of the PFC-Hb circuit in mediating the effects of drugs other than cocaine has not been addressed in the preclinical literature.

Despite its unique role in cocaine addiction, few studies to date have investigated the specific PFC-Hb projection in the human brain, including in human drug addiction (Savjani et al., 2014). A growing body of studies in small animal highlights unequivocal evidence for a monosynaptic medial PFC (mPFC) projection to the Hb (Li et al., 2011; Ye et al., 2016), with roles in regulating socially directed behavior (Benekareddy et al., 2018) and working memory (Mathis et al., 2017). Evidence for such a direct PFC-Hb projection is less consistent in non-human primate tracer studies, although a handful of studies in macaques

do support the existence of a similar PFC-Hb anatomical connection in the primate brain (Cavada et al., 2000; Chiba et al., 2001; Preuss & Goldman-Rakic, 1987). Additionally, the phylogenetically conserved nature of the Hb circuitry (Stephenson-Jones et al., 2012) further motivates the exploration of the PFC-Hb anatomical projection in humans using diffusion magnetic resonance imaging (MRI) tractography (Freudenmacher et al., 2020), taking advantage of the sizable afferent fibers to the Hb through the stria medullaris (SM), a relatively thick fiber bundle situated on the dorsal-medial surface of the thalamus (Sutherland, 1982; Zahm & Root, 2017).

To evaluate the microstructural features of the PFC-Hb connection while avoiding partial volume effects, it is preferred to restrict quantification to a common major fiber pathway. Although the exact anatomical pathway of the PFC-Hb in the human brain is still elusive, the anterior limb of the internal capsule (ALIC), a major fiber bundle that carries thalamic and brainstem tracts to/from the PFC, serves as a highly plausible conduit as indicated by a previous diffusion tractography study seeding from the habenula (Shelton et al., 2012). White matter pathways with different functional origins are topologically organized within the ALIC (Safadi et al., 2018). Importantly, white matter pathology in the ALIC was previously observed in distinct PFC projections in humans with bipolar disorder, suggesting that microstructural hallmarks of disease may be localized to specific tracts in this region (Safadi et al., 2018). Similarly, diffusion tensor imaging (DTI) studies in human drug addiction suggest white matter microstructural abnormalities in the ALIC (He et al., 2020; W. Li et al., 2016) measured with reduced fractional anisotropy (FA), an index of the coherence of the diffusion process that can be used to infer alterations in the underlying tissue architecture in major fiber tracts associated with the PFC (Tondo et al., 2021).

In the present study, we performed probabilistic diffusion MRI tractography using individualized seeds in the Hb and control subcortical regions to assess their topology of structural connections with the PFC. Next, by probing the tissue microstructure using DTI, we aimed to explore white matter microstructural features in the PFC-Hb tract in individuals with cocaine use disorder (CUD), including short-term abstinent (CUD−) and current (CUD+) users, as compared to demographically matched healthy individuals. We additionally tested, for the first time, the generalizability of PFC-Hb circuity impairments to heroin addiction, in a group of inpatient heroin-addicted individuals on medication-assisted treatment. We hypothesized that PFC-Hb white matter microstructure is (1) characterized by reduced coherence, as compared to healthy controls, in individuals with CUD and generalizable to individuals with heroin use disorder (HUD), and (2) associated with drug use severity measures, encompassing recent or chronic use, or premorbid/predisposing factors.

Results

Demographic, psychometric, and drug use variables

Cocaine- and heroin-addicted individuals were recruited along with two groups of healthy control (CTL) subjects, demographically matched to the two addiction groups. Both the CUD and HUD groups were well matched to their respective CTL groups on age, sex, race, and ethnicity, but not on education (CTL > CUD/HUD), verbal (CTL > CUD+/HUD) and

non-verbal (CTL/CUD− > CUD+) intelligence, and depression symptomatology (CTL < CUD/HUD). There were also differences in recent alcohol use (CUD+ > CTL = CUD− > HUD, driven in part by restricted access to alcohol for the inpatient HUD subjects), cigarette smoking (driven by CTL, who were mostly never smokers), and severity of nicotine dependence (CTL < CUD−/HUD) (Table 1). Within the addiction groups, there were differences in race (compared to CUD, the HUD group was comprised of significantly fewer Black and more White participants), ethnicity (more HUD than CUD subjects identified as Hispanic), alcohol use (CUD+ > HUD) and severity of nicotine dependence (CUD+ < HUD). Significant between-group differences were also found for the drug of choice (DOC) for current abstinence duration (CUD+ < CUD− = HUD), past 30-day use (CUD+ > CUD− = HUD), craving (CUD+ = HUD > CUD−) and severity of dependence (CUD+ < CUD− = HUD).

Prefrontal-habenular tracts display distinct topology within and posterior to the ALIC

Prefrontal cortical connections with the Hb, as well as control regions in the anterior thalamus (AT) and ventral tegmental area (VTA) (Figure 1) were modeled by streamline bundles (hereby referred to as a “tract”) generated in the left and right hemisphere with endpoints in each region of interest. Qualitatively, the rending of structural connections prior to entering the ALIC (S2 in Figure 2A) in CUD subjects and their matched CTL group showed a ventral-medial pathway for the Hb streamlines relative to streamlines from the AT and VTA (Figure 2B). Within the ALIC, the Hb streamlines maintain this ventral-medial topology. Such topological distinction was highly consistent across subjects. Quantitatively, the degree of overlap between binarized streamline tracts within the ALIC was less than 70%: for the Hb, 58.6% overlap with AT and 52.9% overlap with VTA; for the AT, 52.2% overlap with Hb and 61.8% overlap with VTA; and for the VTA, 52.8% overlap with Hb and 69.8% overlap with AT (Figure 2C).

Prefrontal-habenular tracts reach distinct prefrontal cortical target

Streamline terminal distributions in the PFC were compared between tracts seeded in each of the subcortical regions of interest (Figure 3A). All three subcortical seed regions produced streamlines terminating in the superior frontal gyrus (SFG), middle frontal gyrus (MFG), inferior frontal gyrus (IFG), and orbitofrontal cortex (OFC) target regions in every individual, whereas fewer than two-thirds of individuals produced any streamlines terminating in the frontal pole (FP) or anterior cingulate cortex (ACC) (Figure 3B). As a result, statistical tests were performed only in the former four regions. The percentage of streamlines projecting from our seed regions of interest to the PFC target regions was analyzed using a 3 (Group: CTL, CUD+, CUD−) × 3 (Seed: Hb, AT, VTA) × 4 (Target: SFG, MFG, IFG, OFC) × 2 (Side: left, right) ANOVA. There was a significant main effect of Target (SFG > MFG > IFG > OFC), $F(3,1344) = 556.45$, $p < .001$, which was qualified by a significant Seed × Target interaction effect, $F(6,1344) = 25.04$, $p < .001$ (Figure 3B). Additionally, there was a significant Group × Target interaction effect, $F(6,1344) = 2.74$, $p = .012$ (Figure 3C). No other main or interaction effects reached significance, $F < 1.14$, $p > .333$. Post hoc analysis of the Seed × Target interaction showed a significant effect of Seed for all four targets and vice versa, implicating highly distinguishable targets in the PFC for the Hb streamlines as compared to the two control seed regions. For the effect of Seed:

SFG (AT = VTA > Hb), $F(2,348) = 40.84$, $p < .001$; MFG (Hb > AT = VTA), $F(2,348) = 7.02$, $p = .001$; IFG (Hb > AT = VTA), $F(2,348) = 3.51$, $p = .031$; and OFC (Hb > AT = VTA) $F(2,348) = 16.28$, $p < .001$. For the effect of Target: Hb (MFG > SFG = IFG > OFC), $F(3,464) = 158.41$, $p < .001$; AT (SFG = MFG > IFG > OFC), $F(3,464) = 244.81$, $p < .001$; and VTA (SFG = MFG > IFG > OFC), $F(2,464) = 211.23$, $p < .001$. Finally, post hoc analysis of the Group × Target interaction showed a significant effect of Group in the MFG, the region containing the most Hb streamline terminals (CTL > CUD+ = CUD−), $F(2,348) = 5.20$, $p = .006$.

Analysis of the Hb streamline terminal distribution was reproduced in the independent HUD sample and demographically matched CTL group using a 2 (Group: CTL, HUD) × 4 (Target: SFG, MFG, IFG, OFC) × 2 (Side: left, right) ANOVA (Figure S1). There was a significant main effect of Target (MFG > SFG = IFG > OFC), $F(3,468) = 153.98$, with no other main or interaction effects reaching significance, $F < 1.72$, $p > .165$.

Microstructural integrity is impaired in PFC-Hb tracts in CUD compared to CTL

For each streamline, DTI measures were extracted from each voxel and averaged with the other streamlines to obtain one value per tract in each hemisphere. The four DTI indices (fractional anisotropy, FA; mean diffusivity, MD; axial diffusivity, AD; and radial diffusivity, RD) were compared separately, correcting for multiple comparisons, using 3 (Group: CTL, CUD+, CUD−) × 2 (Side) ANOVAs in the Hb tracts along the entirety of the streamlines terminating in the PFC, as well as in the AT and VTA tracts as controls (Figure 4A). For FA, this analysis in the Hb tracts revealed a significant main effect of Group (CTL > CUD+ = CUD−), $F(2,112) = 6.06$, $p = .003$, with no other significant main or interaction effects, $F < 0.94$, $p > .333$. This same analysis in the AT or VTA tract did not yield any significant effects after correcting for multiple comparisons, $F < 4.77$, $p > .010$. Additionally, there were no significant main or interaction effects for MD, $F < 2.34$, $p > .101$; AD, $F < 1.66$, $p > .196$; or RD, $F < 3.69$, $p > .028$, in any of the three tracts (Figure S2A).

Additional analyses were performed separately in the ALIC (S2) subsection of each of the tracts to assess the specificity of the DTI metrics in this majority white matter region where the three pathways converge using 3 (Group: CTL, CUD+, CUD−) × 2 (Side) ANOVAs (Figure 4B). For FA, this analysis in the Hb tract revealed a significant main effect of Group (CTL > CUD), $F(2,112) = 6.66$, $p = .002$, with no other significant main or interaction effects, $F < 1.82$, $p > .166$. This same analysis in the AT and VTA tract did not yield any significant results after correcting for multiple comparisons, $F < 4.62$, $p > .012$. Additionally, there were no significant main or interaction effects for MD, $F < 1.16$, $p > .318$; AD, $F < 1.44$, $p > .242$; or RD, $F < 4.70$, $p > .011$ (uncorrected trend), in any of the three tracts (Figure S2B). To assess the segmental specificity of the DTI group effect for FA in the Hb tract, we performed three 3 (Group) × 2 (Side) ANOVAs on FA in S1 and S3 in addition to S2 (see above), with Bonferroni correction for the three separate comparisons (alpha level .05/3 = .017) (Figure 5). This analysis yielded no significant main or interaction effects in either S1 ($F < 0.73$, $p > .484$) or S3 ($F < 1.92$, $p > .152$).

White matter microstructural abnormalities observed in CUD show similar pattern in HUD

Mean FA was compared along the whole tract and in the ALIC subsection using two-sample t-tests in the HUD and its age, sex, race, and ethnicity-matched CTL group (Figure 6A). In the whole tract, this analysis yielded a significant group difference, $t(39) = 2.60$, $p = .013$ (CTL > HUD). However, no group difference was observed in the ALIC, $t(39) = 0.72$, $p = .476$. Additionally, for comparison of the three substance use disorder groups, a 3-way (Group: CUD+, CUD−, HUD) ANOVA revealed no significant main effect of Group in the whole tract or in the ALIC, $F(2,52) < 1.40$, $p > .255$ (Figure 6B).

Lower FA is correlated with younger age of first use in drug-addicted individuals

Given a similar magnitude of PFC-Hb whole tract FA decreases across the addiction groups as compared to CTL groups, which was observed despite variability in several DOC measures, we combined the CUD+, CUD−, and HUD groups to assess correlations with the drug use variables that did not differ between the groups (i.e., age of first use, duration of regular use, and withdrawal) (Table 1). This analysis revealed a significant correlation with age of first use, $r = 0.30$, $p = .025$ (Figure 7). This effect remained significant when including as a covariate in the linear regression model individuals' years of regular use, $p = .023$, which was correlated with age of onset, $r = 0.31$, $p = .022$. No significant correlations were observed for duration of regular use, $p = .652$, or withdrawal, $p = .665$.

Discussion

For the first time in the human brain, we present consistent evidence for a plausible PFC-Hb tract with specific impairments in both cocaine and heroin addiction. Motivated by the specificity of the PFC-Hb projection results, we quantitatively evaluated the microstructure of this pathway in currently using and short-term abstinent cocaine-addicted individuals. In support of our first hypothesis, the PFC-Hb tract displayed decreased FA in both these addicted subgroups compared with healthy controls, which was driven by the microstructural impairment of the ALIC. Importantly, results demonstrated a similar reduction in FA across the whole PFC-Hb tract in a separate cohort of heroin-addicted individuals compared to their own demographically matched healthy control subjects, in a pattern that was indistinguishable from the CUD group. Consistent with our second hypothesis, across all cocaine- and heroin-addicted subjects, and in an exploratory analysis, greater white matter impairment in the whole tract was associated with a younger age of first use of the individuals' drug of choice. This result may suggest a common predisposing role (or impairments associated with early life drug use) for the microstructural integrity of the PFC-Hb tract in the development of substance use disorders.

Although the existence of the PFC-Hb tract in the primate brain is not well established, tracer studies in macaques with relatively broad cortical coverage of the anterograde tracer injection sites, specifically from (i) Brodmann area 32/25/24b (Chiba et al., 2001), (ii) OFC (Cavada et al., 2000), and (iii) Brodmann area 9/10 (Preuss & Goldman-Rakic, 1987), show evidence of direct anatomical connectivity to the Hb. Further, a growing body of small animal evidence points to an unequivocal monosynaptic medial PFC-LHb projection (Benekareddy et al., 2018; Li et al., 2011; Mathis et al., 2021; Ye et al., 2016), which is

consistent with the preferential MFG termination of our Hb streamline results (Mathis et al., 2017). In addition, the ventromedial topological feature of our PFC-Hb tract is consistent with the well-known, phylogenetically conserved midline orientation of the Hb circuit (Ely et al., 2019; Zahm & Root, 2017). This converging evidence prompted us to adopt the term “PFC-Hb tract” to describe our current noninvasive neuroimaging results.

Studies using voxel-wise whole-brain analysis methods have previously reported white matter abnormalities, mostly in the form of diffuse reductions in FA encompassing major cortical tracts (superior longitudinal fasciculus, corpus callosum, and anterior thalamic radiations), in cocaine addiction (Azadeh et al., 2016; He et al., 2020; Ma et al., 2017) (although some, mostly earlier, studies have also reported increases in FA) (Bell et al., 2011; Romero et al., 2010; Vaquero et al., 2017). Similar results, notably in fiber tracts associated with frontal brain regions, were also reported in heroin users (Li et al., 2013; Liu et al., 2008; Wang et al., 2013; Wollman et al., 2015). As compared to these major white matter tracts in these voxel-wise mapping studies, our results highlight a similar microstructural abnormality in a previously unexplored and small, yet highly conserved, white matter tract between the frontal lobe and the Hb.

The link between cocaine use and abnormalities in white matter FA is consistent with cocaine-induced neurotoxicity and neuroinflammatory effects, including reactive gliosis, which may disrupt the microarchitectural organization of axon bundles especially in subcortical regions (Clark et al., 2013; Tondo et al., 2021). Neurotoxic mechanisms are also linked to heroin use, including induced neuronal apoptosis, mitochondrial dysfunction, and reduced blood-brain barrier structural integrity (Pimentel et al., 2020; Tian et al., 2017). Disruptions in oligodendrocyte proliferation and the expression of myelin-related genes can further explain heroin-induced white matter abnormalities specifically in the PFC (Martin et al., 2018). Additional mechanisms underlying the white matter alterations in cocaine addiction may encompass elevated risk for cerebrovascular events, including ischemic and hemorrhagic stroke, as has been previously reported in frequent cocaine users, notably in the cerebral arteries that supply the subcortical white matter (Cheng et al., 2016; Kaufman et al., 1998; Martin-Schild et al., 2010). Increased vasoconstriction can also potentially impact the myelination and structural integrity of axons in the affected fiber bundles (Montoya-Filardi & Mazon, 2017). Although the direct measurement of these physiological processes on a microscopic scale is not possible with DTI, in a rodent model of cocaine addiction reduced white matter FA and increased RD were specifically colocalized with myelin damage and destabilized neurite outgrowth in the internal capsule and the corpus callosum (Narayana et al., 2014). Our results in the CUD groups showing significantly decreased FA, driven by the ALIC of PFC-Hb tracts, in combination with a trend towards increased RD ($p = .011$, uncorrected), may similarly reflect greater axonal dispersion or lower packing density resulting in less coherent directionality of the diffusion along these pathways.

Similar FA reductions in the independent sample of heroin-addicted individuals implicates the physiological importance of this pathway not only to stimulants, as has been previously demonstrated in rodent models, but in opiate addiction as well. Combined with the correlation with drug use across all addicted subjects, such that greater severity of white matter effects was associated with younger age of first drug use, these results suggest

that this microstructural deficit in the PFC-Hb may be a core marker in drug addiction, potentially indicative of vulnerability factors that contribute to (or reflect) the development and maintenance of the addiction cycle. Notably, early exposure to drugs of abuse such as cocaine and heroin during adolescence has been shown to impact neurodevelopment, especially in the PFC and limbic system (Jordan & Andersen, 2017; Squeglia et al., 2009). Nevertheless, the differential pattern of results (specificity to the ALIC in CUD, which was not observed in HUD) is suggestive of multiple potential addiction-related processes affecting the white matter microstructure in this tract. The exploratory results suggesting a correlation with age of onset remain to be replicated with corrections for multiple comparisons and in larger sample sizes. Furthermore, polysubstance use is highly prevalent in the clinical populations studied here, and we acknowledge that group differences in the use of substances other than cocaine and heroin (e.g., alcohol, cannabis, and nicotine) may have contributed to the observed white matter effects. However, it is important to note that all other substance use disorders were in sustained remission at the time of the study, and measures of recent alcohol and nicotine use were found to not be associated with our variables of interest (analyses not possible for cannabis as only four subjects reported any past 30-day cannabis use).

Our streamline termination results suggest that, compared with the other subcortical regions examined, the Hb exhibits stronger connectivity with the cortical regions that are associated with decision-making and inhibitory control (i.e., the OFC, IFG, and MFG), which supports further interrogation of the functional significance of Hb connectivity in addiction. Our SFG, MFG, IFG, and OFC results are largely consistent with strong connections found in another diffusion tractography study seeding from the cortex to the habenula; while our FP and ACC results stand largely in contrast to findings in that study (Vadovičová, 2014). Unfortunately, in a similar diffusion tractography study seeding from the habenula, PFC–Hb connectivity results were not reported in sufficient detail for comparison (Shelton et al., 2012). These discrepancies with prior literature highlight the importance of technical details in the tractography analysis, as well as diffusion MRI data quality and resolution. As an incidental finding (not correlated with our main results), we also observed reduced streamline terminal density in the MFG relative to the other PFC subregions for all three subcortical seed regions of interest in both CUD groups (Figure 3C, MFG). The dorsolateral PFC, which is located within the MFG, serves important roles in learning, memory, and higher order executive functions such as cognitive control/shifting, is frequently reported in relation to core deficits in impulse control and salience attribution in drug addiction (Goldstein & Volkow, 2011), and is often used as a direct stimulation target to reduce craving in CUD (e.g., (Gaudreault et al., 2021)). However, the anatomical connectivity profile of the dorsolateral PFC in humans has yet to be fully characterized. Further investigation of the possible role of dorsolateral PFC-limbic connectivity in drug addiction is nevertheless warranted.

With limited tracer studies available in nonhuman primates to date, we recognize the on-going debates as to the existence, as well as the precise anatomical location, of the intended fiber pathways analyzed in this study. A careful replication of the tracer studies in macaques would be needed for a strict neuroanatomical validation of whether the PFC-Hb pathway is conserved in the human brain. Instead, we used human neuroimaging with 3T MRI to perform, for the first time, tractography from three separate subcortical seed regions to

cortical targets. The tissue composition of these subcortical seeds is complex, as are the axonal projections/terminals associated with these structures. This is further complicated by the limited image resolution of in vivo diffusion tractography, especially where different tracts organize as they leave the ALIC to reach a mixture of targets. As a result, the three tracts in this study may inevitably be contaminated by adjacent structures that project to/from the PFC through the ALIC. Specifically, our neuroimaging-defined PFC-Hb tract probably includes neuroanatomical projections in the dorsal-posterior direction at the level of the thalamus, which may contain the medial mediodorsal thalamic nucleus, although to the best of our knowledge there is no evidence that this region receives projections through the SM (Roddy et al., 2018; Sutherland, 1982). Furthermore, our PFC-VTA tract likely represents multiple ascending neuroanatomical projections from the inferior direction in the brainstem. It is important to note that we do not claim an ALIC pathway for this tract, but rather we leverage the consistent diffusion tractography result of ascending VTA fibers through the ALIC, which have been labeled “false positive” (Haber et al., 2022) yet are of help, given their topology, in distinguishing this population of streamlines from those from the other two seeds)], and the PFC-AT tract may also include projections from other thalamic nuclei passing through the AT. Importantly, diffusion tractography is not a ground truth for neuroanatomy, providing instead an estimate of the path of probable structural connectivity between brain regions, which is influenced by actual white matter pathways but also the quality of the diffusion MRI and technical details of the tractography analysis (Jbabdi et al., 2015). Acknowledging this inevitable gap between in vivo diffusion tractography and the underlying neuroanatomy, the strong topological consistency of our results nevertheless adds important new information to the field, urging further postmortem studies in non-human primates of the PFC-Hb tract (Yendiki et al., 2022).

The imaging acquisition methods and resolution employed here also prohibited separate segmentation of the lateral and medial Hb, both displaying notable functional distinctions in the context of addiction (Velasquez et al., 2014). Ultra-high resolution multi-shell diffusion MRI acquisition methods may allow for greater precision in tract estimation by reducing the potential for contamination from medial Hb fibers (Strotmann et al., 2014). Nevertheless, PFC input to the Hb terminates exclusively in the lateral nucleus (Mizumori & Baker, 2017), which supports our decision to emphasize functions attributed to the LHb. A more complete interrogation of the Hb circuitry, including its connections to the dopaminergic and serotonergic midbrain, will be vital for understanding the downstream effects of impaired PFC connectivity on the structure and functioning of the larger reward system. Additionally, future studies should include more women to adequately assess the potential for sex differences in white matter microstructure (Ritchie et al., 2018) in drug addiction. Finally, our interpretation of direct comparisons between substance use disorders was limited by key differences between the SUD subgroups, especially in treatment status. These differences were partially accounted for by subdividing the CUD group based on their urine toxicology results/length of abstinence, such that the CUD+ group controlled for current drug use and the CUD− for time since last use (which did not differ from that of HUD). Nevertheless, these important comparisons were limited by the small sample size, prohibiting the detection of interesting trends in the data (e.g., most FA decreases in the CUD−). Future studies may benefit not only from larger samples but also from a longitudinal design, as well as the

inclusion of both currently using and opioids-abstinent heroin-addicted individuals, to better discriminate the effects of current use vs. abstinence and recovery on the integrity of the PFC-Hb projection in drug addiction. For example, microstructural impairment in a tract associated with the nucleus accumbens was recently shown to predict relapse in individuals with stimulant use disorder (Tisdall et al., 2022), further highlighting the importance of better understanding the putative relationship between white matter and recovery.

In summary, using in vivo diffusion tractography we found a topologically distinct fiber pathway between the PFC and Hb in the human brain that parallels the PFC-Hb projections reported in small animal studies. Using DTI measures obtained specifically along this PFC-Hb projection, we show microstructural impairments in individuals with CUD as generalized to a separate cohort of heroin-addicted individuals and commonly showing a greater deficit with earlier drug use onset. Overall, our results advance ongoing research in the field by targeting a previously unexplored circuit in the pathophysiology of addiction in humans, where deficits may predispose both to the development of drug addiction and to relapse, as potentially amenable for individually tailored prevention efforts and/or treatment.

Methods

Resource Availability

Lead Contact—Further information and requests for resources should be directed to and will be fulfilled by the lead contact, Rita Z. Goldstein (rita.goldstein@mssm.edu).

Materials Availability—This study did not generate new unique reagents.

Data and Code Availability

- All data reported in this paper will be shared by the lead contact upon request.
- This paper does not report original code.
- Any additional information required to reanalyze the data reported in this paper is available from the lead contact upon request.

Experimental Model and Subject Details

Participant Recruitment—Thirty-one individuals with cocaine use disorder (CUD) and 29 healthy control (CTL) subjects were included in this study. An additional cohort of 24 individuals with heroin use disorder (HUD) and 17 CTL subjects was also included. Data from these subjects (except HUD-matched CTL subjects) are also included in a separate analysis of white matter using tract-based spatial statistics in substance use disorder (Gaudreault et al., 2022). Compared to this other study, the current study employed methods suitable for modeling precise structural connections that cannot be otherwise analyzed using whole-brain methods, which included both T1 and T2-weighted scans in addition to diffusion weighted imaging (DWI) and a fiber orientation diffusion function (fODF) pipeline to assess specific WM fiber bundles. Both subjects with CUD and HUD were recruited by advertisements and flyers (in local newspapers, bulletin boards, and online) as well as through educational talks provided to staff and patients groups at collaborating substance

abuse prevention and treatment organizations in the New York City metropolitan area. Using a similar approach (advertisements and flyers), the healthy controls were recruited from the same communities for matching purposes. Decisions about participant inclusion for all groups were made by the same senior clinical psychologists. Cocaine-addicted individuals were considered for inclusion if they had a history of substance use disorder (SUD) with cocaine as their primary drug of choice (DOC) as assessed with the Structured Clinical Interview for the *Diagnostic and Statistical Manual of Mental Disorders, Fourth Edition* (SCID-IV) (First et al., 1997). All heroin-addicted participants were inpatients in a single drug addiction rehabilitation facility (Samaritan Daytop Village, NY) on medication-assisted treatment; they met criteria for SUD with heroin as their primary DOC as assessed with the Mini International Neuropsychiatric Interview (Sheehan et al., 1998). The Addiction Severity Index (McLellan et al., 1992) was part of the diagnostic interview for all SUD subjects. Symptoms of withdrawal, craving, and severity of dependence were evaluated with the Cocaine Selective Severity Assessment (Kampman et al., 1998) or Short Opiate Withdrawal Scale (Gossop, 1990), the 5-item Cocaine Craving Questionnaire (Tiffany et al., 1993) or 14-item Heroin Craving Questionnaire (Heinz et al., 2006), and the Severity of Dependence Scale (Gossop et al., 1995), respectively. Scores for withdrawal and craving were range-corrected to allow for group comparisons.

All participants underwent a brief physical examination including breath carbon monoxide (for cigarette smoking) and alcohol measurements, and a review of medical history. Cigarette use and nicotine dependence were also assessed with the Fagerstrom Test for Nicotine Dependence (Heatherton et al., 1991). A urine toxicology test was used as an objective assessment of drug use recency, which was further used to classify the CUD group as current users/cocaine urine-positive (CUD+) or abstinent users/cocaine urine-negative (CUD−) to control for the different stages of addiction. Self-reported abstinence duration was consistent with the urine toxicology results in the CUD+ (average 3.3 days since last cocaine use) and CUD− (average 89.6 days) groups (Table 1). All participants in the HUD group were under medication-assisted treatment, with urine toxicology positive for: methadone (n = 19), buprenorphine (n = 4), or both methadone and buprenorphine (n = 1). The mean current self-reported abstinence duration on the day of the MRI scan was four and a half months for the HUD group, matching that of the CUD−. The route of drug administration included smoking (CUD n = 28; HUD n = 3), intra-nasal (CUD n = 23; HUD n = 17), intravenous (CUD n = 2; HUD n = 17) and oral (CUD n = 1; HUD n = 1). Verbal and non-verbal intelligence were estimated using the reading subtest of the Wide Range Achievement Test 3 (WRAT-3) (Jastak & Wilkinson, 1993) and the Matrix Reasoning subtest of the Wechsler Abbreviated Scale of Intelligence (WASI) (Wechsler, 1999), respectively. Participant characteristics are summarized in Table 1.

Comorbidities and Participant Inclusion/Exclusion—The original sample included 37 individuals with CUD and 37 demographically matched CTL subjects, as well as an additional group of 31 individuals with HUD and 24 CTL. Comorbidities among CUD and HUD participants included alcohol use disorder (CUD n = 13; HUD n = 3), cannabis use disorder (CUD n = 5; HUD n = 2), opiate use disorder for CUD (n = 5), cocaine use disorder for HUD (n = 8), polysubstance use disorder (CUD n = 2; HUD n = 2), and post-traumatic

stress disorder (CUD $n = 1$; HUD $n = 1$). All SUD comorbidities were in partial or sustained remission at the time of the study. The CTL participants did not meet criteria for any of these disorders. Individuals who were assessed with the SCID-IV were considered to meet criteria for SUD if the diagnostic criteria were met for either substance abuse or dependence. Polysubstance use disorder was defined for all participants based on the DSM-IV criteria. The CTL participants completed all interviews and questionnaires except instruments that were specific to individuals with a substance use disorder (e.g., assessments of withdrawal, craving, and severity of dependence).

Across all subjects, exclusion criteria were (1) history of head trauma with loss of consciousness (30 minutes or longer), or any neurological disease; (2) abnormal vital signs at the time of screening; (3) current medical illness including cardiovascular disease (e.g., high blood pressure), as well as metabolic, endocrinological, oncological or autoimmune diseases, and infectious diseases common in individuals with SUD including Hepatitis B and C or HIV/AIDS; (4) history of major psychotic (e.g., schizophrenia), neurodevelopmental (e.g., autism), or psychiatric disorders, with the exception of disorders of high comorbidity with SUD for the CUD and HUD groups (e.g., post-traumatic stress disorder, polysubstance use disorder) and nicotine/caffeine dependence for all participants; (5) severe levels of self-reported depression as assessed using the Beck Depression Inventory (Beck et al., 1996) (scores > 20); (6) positive breathalyzer test for alcohol or positive urine screen for any psychoactive drugs, with the exception of cocaine in CUD participants and opioids used for medication-assisted treatment in HUD participants; (7) current use of any medication that may affect neurological functions, with the exception of opioids used for medication-assisted treatment in HUD (antidepressant use in the HUD group was also non-exclusionary); (8) MRI contraindications including any metallic implants, pacemaker device, or pregnancy; and (9) for CTL participants, a positive breathalyzer test for alcohol, positive urine screen for any psychoactive drugs, or history of any SUD.

Further decisions on participant exclusions were made based on MRI quality assurance. Scans were excluded based on excessive motion artifact in diffusion-weighted images ($n = 1$ CUD; $n = 1$ CTL); signal dropout in anterior cortical regions ($n = 2$ CUD); and incidental findings as indicated by a radiologist ($n = 1$ CTL; $n = 1$ HUD). Scans from which tractography streamlines were successfully generated in the primary tract of interest (endpoints in habenula (Hb) and prefrontal cortex (PFC)) were included in further analyses for a final sample of $n = 55$ CTL (28 CUD-matched/17 HUD-matched), $n = 31$ CUD (16 CUD+/15 CUD−), and $n = 24$ HUD (i.e., insufficient streamlines were generated for $n = 14$ CTL, $n = 3$ CUD, and $n = 6$ HUD).

Methods Details

MRI Acquisition—MRI scans were obtained using a Siemens 3.0 Tesla Skyra (Siemens Healthcare, Erlangen, Germany) with a 32-channel head coil. Diffusion-weighted spin-echo EPI images were acquired with opposite phase encoding along the left-right axis, monopolar diffusion encoding with 128 gradient directions (64 in each phase encoding direction) and 13 b=0 scans (1.8 mm isotropic resolution; repetition time 3650 ms; echo time 87 ms; bandwidth 1485 Hz/pixel; single shell maximum b value 1500 s/mm^2, multiband factor

= 3, no in-plane acceleration). T1-weighted (T1w) structural scans were acquired using an MPRAGE sequence (0.8 mm isotropic resolution; repetition time 2400 ms; echo time 2.07 ms; inversion time 1000 ms; flip angle 8°; bandwidth 240 Hz/pixel). T2-weighted (T2w) structural scans were acquired using a SPACE sequence (0.8 mm isotropic resolution; repetition time 3200 ms; echo time 565 ms; bandwidth 680 Hz/pixel).

Structural Data Preprocessing—T1-weighted structural scans were rigidly aligned with each subject's preprocessed b0 scan using FSL's FLIRT for preprocessing with the Freesurfer version 6.0 recon-all pipeline (Fischl et al., 2002), which includes steps for motion correction, non-uniform intensity normalization, skull stripping, and automated segmentation and parcellation based on the Desikan-Killiany atlas (Desikan et al., 2006). The PFC target regions of interest were constructed from parcellations of the superior frontal gyrus (SFG); rostral and caudal middle frontal gyrus (MFG); inferior frontal gyrus (IFG), which contained the pars opercularis, pars orbitalis, and pars triangularis; medial and lateral orbitofrontal cortex (OFC); frontal pole (FP); and rostral and caudal anterior cingulate cortex (ACC).

Segmentation of Subcortical Seed Regions and Inclusion Mask—Segmentation of the Hb was performed semi-automatically by exploiting the structure's high myelin content relative to surrounding tissue as developed and validated for this purpose and described previously (Kim et al., 2016) (Figure 1A). Briefly, each subject's T2w image was co-registered to the T1w image, and T1w-over-T2w images were generated to obtain myelin contrast maps (Glasser & van Essen, 2011). Two individual voxels centered in the left and right Hb region were manually specified, and boundaries were determined automatically by a region growing algorithm with partial volume estimation in the subject's T1w and T2w images and myelin map. Following visual inspection to ensure anatomical validity, the segmented Hb volumes were shape-optimized and downsampled to individuals' diffusion MRI space similar to previously described methods for functional MRI analysis (Ely et al., 2019).

To enhance the anatomical accuracy of the estimated Hb streamlines and filter out streamlines originating in adjacent structures including the mediodorsal thalamus, an intermediate inclusion mask was designated in the most anterior aspect of the stria medullaris (SM). Selection of the inclusion region was performed in the sagittal plane and guided by the T1w-over-T2w image (Figure 1A, right). A 2 × 2 × 2 voxel region in the resolution of the diffusion space was manually drawn in both hemispheres immediately posterior to the anterior columns of the fornix along the third ventricle.

The area around the inclusion mask contains a handful other fiber pathways, including the anterior thalamic radiations and superolateral medial forebrain bundle. In order to evaluate the specificity of the Hb tractography results, we chose two control seed regions for these respective tracts: the anterior thalamus (AT), which was extracted using Freesurfer's anteroventral and ventral anterior thalamic nuclei segmentations, which are fully automated in native space (Iglesias et al., 2018) (Figure 1B); and the ventral tegmental area (VTA), which was generated using a previously established atlas of midbrain structures in MNI space (Murty et al., 2014), thresholded at 0.6 to improve specificity, and coregistered to each

subject's b0 scan (Figure 1C). This atlas is based on manually drawn anatomical tracings with clear anatomical delineations, now the current gold standard for midbrain segmentation in structural MRI. While we employed a combination of manual and atlas-based methods in region of interest selection, all segmentations were visually inspected in native space for each scan to ensure their anatomical validity.

Diffusion Data Preprocessing—Diffusion-weighted images were denoised and preprocessed using the *dwipreproc* command in MRtrix3 (Smith et al., 2004), which incorporates FSL tools to correct for eddy current, motion, and susceptibility-induced distortions (Andersson et al., 2003; Andersson & Sotiropoulos, 2016). Motion and eddy current outlier slices, defined by FSL's eddy, accounted for less than one percent of the total acquired data in all groups (CUD: 0.346 ± 0.49%; CUD-matched CTL: 0.081 ± 0.15%; HUD: 0.606 ± 0.67%; HUD-matched CTL: 0.398 ± 0.42%). Other corrections were made for B1 field inhomogeneity, and intensity normalization was performed (Tustison et al., 2010). Preprocessed diffusion-weighted images were subsequently upsampled to 1.25 mm isotropic voxel resolution. Estimation of the white matter fiber orientation distribution (FOD) function was conducted using the single shell, multi-tissue constrained spherical deconvolution model (Jeurissen et al., 2014; Tournier et al., 2007). For microstructure analysis of DTI measures, the diffusion tensor was fitted locally in each voxel to generate whole-brain maps of the FA (an index reflecting the coherence of diffusion), MD (the bulk averaged/total magnitude of diffusion in all measured directions), AD (the magnitude of diffusion in the primary direction), and RD (the averaged magnitude of diffusion in the secondary and tertiary orthogonal directions) using the FSL function *dtifit* (Woolrich et al., 2009). Note that MD may be linked to neurite dispersion and the intracellular space, AD is associated with axon caliber and fiber density, and RD has been previously shown to correlate with histological markers of demyelination (Alexander et al., 2007).

Tractography—Probabilistic tractography was carried out in MRtrix3 using the Second-order Integration over Fiber Orientation Distributions (iFOD2) algorithm (Tournier et al., 2009) in the upsampled individual subject space. Each subject's FOD map was seeded at random within the left and right Hb volumes (and the control regions: AT and VTA) with a step size of 0.9 mm, with 100 streamlines terminating at the grey/white matter boundary of the PFC selected per hemisphere. Since, to the best of our knowledge, there are no previous reports indicating the existence of direct contralateral input to the Hb (Sutherland, 1982), the contralateral hemisphere was used as an exclusion region. Parameters for streamline selection were an FOD amplitude threshold of 0.15; 400 mm maximum length; and 20° maximum angle between successive steps. The Anatomically Constrained Tractography framework was included to improve the biological validity of streamline estimates using anatomical priors derived from the 5-tissue type segmented T1-weighted image (Smith et al., 2012), with the additional restriction to the SM inclusion mask for Hb streamlines. Individual tracts were visually inspected to ensure all endpoints were located exclusively in the Hb and PFC and streamlines that were irrelevant to the intended analysis (e.g., extending posterior or inferior to the Hb through the fasciculus retroflexus) were removed. Tracts from the Hb were segmented into subsections S1, S2, and S3 to assess potential spatial differences in the tissue microstructure in pre-specified anatomical sections. Boundaries

were designated in the coronal plane as follows: for S1, immediately anterior to the Hb extending to the anterior SM inclusion mask as described above; for S2, immediately anterior to the genu of the internal capsule extending to the most anterior slice containing the caudate (encompassing the ALIC); and for S3, immediately anterior to the caudate extending to the PFC grey/white matter boundary (Figure 2A). For all tracts, DTI measures were extracted from each voxel along every streamline, and streamline means were averaged across all voxels and between both hemispheres to produce one value per tract for each subject.

For the control regions, streamlines seeded from the VTA were restricted to pass through the ALIC, or S2, as defined above, with exclusion regions in the AT and in the brainstem immediately inferior to the VTA to eliminate overlap with adjacent structures. Streamlines seeded from the AT were restricted to pass through the same ALIC inclusion region. To quantify the spatial distinction between Hb and control streamlines in the ALIC, tracts in this region were binarized in each subject's T1w space. Spatial overlap between the three tracts was computed for each of the three subcortical seed regions as the percentage of the total mask volume contained within each of the other masks, averaged between left and right hemispheres (e.g., the percentage of voxels within the Hb tract mask that also contain streamlines from the AT) (Figure 2C).

Finally, although tractography was performed with subcortical seed regions and the PFC as the target region, considering that anatomical connectivity with the Hb is unidirectional from the PFC, and tractography is indifferent to directionality, we refer to these projections as "PFC-Hb tracts" to uphold consistency with the previously established anatomy.

Quantification and Statistical Analysis

Group comparisons for demographic and drug use measures were performed using chi-square tests for categorical variables, while continuous variables were analyzed using Student's *t* tests or non-parametric Mann-Whitney U for normal and non-normal distributions, respectively. A comparison of streamline distributions (percent of streamline endpoints) was performed using a 3 (Group: CTL, CUD+, CUD−) × 3 (Seed: Hb, AT, VTA) × 4 (Target: SFG, MFG, IFG, OFC) × 2 (Side: left, right) ANOVA. Group differences in white matter microstructure in each of the three subcortical seed regions were analyzed for each of the four DTI measures with 3 (Group: CTL, CUD+, CUD−) × 2 (Side: left, right) ANOVAs. For these DTI analyses, Bonferroni correction for multiple comparisons was used with an alpha level of .05/12 = .004 to account for four (FA, MD, AD, RD) separate analyses in the three tracts. Additionally, these same analyses were performed separately in S2 to assess specificity in the region of the ALIC where functionally segmented white matter pathways converge yet still maintain topological distinction; we then used as the dependent measure any DTI metrics that survived our multiple comparisons-corrected significance testing in a 3 (Group: CTL, CUD+, CUD−) × 2 (Side: left, right) ANOVA. The same statistical test was performed separately for the other two subsections (S1 and S3) to assess the spatial distribution of any significant DTI effects. Dependent DTI metrics that showed significant group effects (between CUD and CTL) were averaged between the left and right hemisphere in the absence of laterality effects and inspected in HUD using a two-sample

t-test with their own matched CTL, followed by a 3-way (Group: CUD+, CUD−, HUD) ANOVA. ANOVA statistics for the main group comparisons of interest are presented in Table S1. For all ANOVAs, significant main effects were followed up with Tukey HSD post hoc tests and simple effects analyses were performed to follow any significant interaction effects. To control for potential covariates, the effects of any demographic, psychometric and non-DOC drug use variables that differed between the groups were inspected for their associations with the DTI metrics exhibiting significant group differences (see Table 1). None of these tests were significant and, therefore, no covariates were included in the analyses. We also assessed correlations between our dependent DTI metrics that showed significant group effects with drug use and addiction severity variables (for the DOC). Three variables that did not differ significantly between the addicted groups were assessed as measures of lifetime use (duration of regular use), current severity (withdrawal), and possible predisposing factors (age of first use). Due to the exploratory nature of the analysis of drug use variables, statistical tests were not corrected for multiple comparisons. All statistical tests were performed using R version 3.6.1 (R Core Team, n.d.).

Supplementary Material

Refer to Web version on PubMed Central for supplementary material.

Acknowledgments:

We appreciate the thoughtful discussions with our colleagues, Drs. Patrick Hof, Mark Baxter, Paul Kenny, and Peter Rudebeck, in the Department of Neuroscience at the Icahn school of Medicine at Mount Sinai. We are equally grateful to Dr. Suzanne Haber, in the Department of Psychiatry at Harvard Medical School, and Dr. Sarah Heilbronner, in the Department of Neuroscience at University of Minnesota, for in-depth neuroanatomical discussions. This work was funded by the Canadian Institutes of Health Research Postdoctoral Research Fellowship (P-O.G.), NIDA R01 DA041528 (R.Z.G.), NIDA R01 DA04830 (R.Z.G.), NIDA R21 DA034954 (R.Z.G.), and NCCIH R01 AT010627 (R.Z.G.).

Inclusion and Diversity:

We worked to ensure gender balance in the recruitment of human subjects. We worked to ensure ethnic or other types of diversity in the recruitment of human subjects. We worked to ensure that the study questionnaires were prepared in an inclusive way.

References

Alexander AL, Lee JE, Lazar M, & Field AS (2007). Diffusion Tensor Imaging of the Brain. Neurotherapeutics, 4(3). 10.1016/j.nurt.2007.05.011

Andersson JLR, Skare S, & Ashburner J (2003). How to correct susceptibility distortions in spin-echo echo-planar images: Application to diffusion tensor imaging. NeuroImage, 20(2), 870–888. 10.1016/S1053-8119(03)00336-7 [PubMed: 14568458]

Andersson JLR, & Sotiropoulos SN (2016). An integrated approach to correction for off-resonance effects and subject movement in diffusion MR imaging. NeuroImage, 125, 1063–1078. 10.1016/j.neuroimage.2015.10.019 [PubMed: 26481672]

Azadeh S, Hobbs BP, Ma L, Nielsen DA, Gerard Moeller F, & Baladandayuthapani V (2016). Integrative Bayesian analysis of neuroimaging-genetic data with application to cocaine dependence. NeuroImage, 125. 10.1016/j.neuroimage.2015.10.033

Beck AT, Steer RA, & Brown GK (1996). Manual for the Beck depression inventory-II. San Antonio, TX: Psychological Corporation.

Bell RP, Foxe JJ, Nierenberg J, Hoptman MJ, & Garavan H (2011). Assessing white matter integrity as a function of abstinence duration in former cocaine-dependent individuals. Drug and Alcohol Dependence, 114(2–3). 10.1016/j.drugalcdep.2010.10.001

Benekareddy M, Stachniak TJ, Bruns A, Knoflach F, von Kienlin M, Künnecke B, & Ghosh A (2018). Identification of a Corticohabenular Circuit Regulating Socially Directed Behavior. Biological Psychiatry, 83(1), 607–617. 10.1016/j.biopsych.2017.10.032 [PubMed: 29336819]

Cavada C, Compañy T, Tejedor J, Cruz-Rizzolo RJ, & Reinoso-Suárez F (2000). The anatomical connections of the macaque monkey orbitofrontal cortex. A review. Cerebral Cortex, 10(3). 10.1093/cercor/10.3.220

Cheng YC, Ryan KA, Qadwai SA, Shah J, Sparks MJ, Wozniak MA, Stern BJ, Phipps MS, Cronin CA, Magder LS, Cole JW, & Kittner SJ (2016). Cocaine use and risk of ischemic stroke in young adults. Stroke, 47(4). 10.1161/STROKEAHA.115.011417

Chiba T, Kayahara T, & Nakano K (2001). Efferent projections of infralimbic and prelimbic areas of the medial prefrontal cortex in the Japanese monkey, Macaca fuscata. Brain Research, 888(1), 83–101. 10.1016/S0006-8993(00)03013-4 [PubMed: 11146055]

Clark KH, Wiley CA, & Bradberry CW (2013). Psychostimulant abuse and neuroinflammation: Emerging evidence of their interconnection. Neurotoxicity Research, 23(2). 10.1007/s12640-012-9334-7

Desikan RS, Ségonne F, Fischl B, Quinn BT, Dickerson BC, Blacker D, Buckner RL, Dale AM, Maguire RP, Hyman BT, Albert MS, & Killiany RJ (2006). An automated labeling system for subdividing the human cerebral cortex on MRI scans into gyral based regions of interest. NeuroImage, 31(3), 968–980. 10.1016/j.neuroimage.2006.01.021 [PubMed: 16530430]

Ely BA, Stern ER, Kim J, Gabbay V, & Xu J (2019). Detailed mapping of human habenula resting-state functional connectivity. NeuroImage, 200, 621–634. 10.1016/j.neuroimage.2019.06.015 [PubMed: 31252057]

First M, Spitzer R, Gibbon M, & Williams J (1997). User's Guide for the Structured Clinical Interview for DSM-IV Axis I Disorders SCID-I: Clinician Version. American Psychiatric Pub.

Fischl B, Salat DH, Busa E, Albert M, Dieterich M, Haselgrove C, van derKouwe A, Killiany R, Kennedy D, Klaveness S, Montillo A, Makris N, Rosen B, & Dale AM (2002). Whole brain segmentation: Automated labeling of neuroanatomical structures in the human brain. Neuron, 33(3), 341–355. 10.1016/S0896-6273(02)00569-X [PubMed: 11832223]

Freudenmacher L, von Twickel A, & Walkowiak W (2020). The habenula as an evolutionary conserved link between basal ganglia, limbic, and sensory systems—A phylogenetic comparison based on anuran amphibians. Journal of Comparative Neurology, 528(5). 10.1002/cne.24777

Gaudreault P-O, Sharma A, Datta A, Nakamura-Palacios EM, King S, Malaker P, Wagner A, Vasa D, Parvaz MA, Parra LC, Alia-Klein N, & Goldstein RZ (2021). A double-blind sham-controlled phase 1 clinical trial of tDCS of the dorsolateral prefrontal cortex in cocaine inpatients: Craving, sleepiness, and contemplation to change. European Journal of Neuroscience, 53(9). 10.1111/ejn.15172

Gaudreault P-O, King S, Malaker P, Alia-Klein N, & Goldstein RZ (2022). Generalized and specific whole-brain white matter abnormalities in human cocaine and heroin use disorders. MedRxiv.

Gill MJ, Ghee SM, Harper SM, & See RE (2013). Inactivation of the lateral habenula reduces anxiogenic behavior and cocaine seeking under conditions of heightened stress. Pharmacology Biochemistry and Behavior, 111, 24–29. 10.1016/j.pbb.2013.08.002 [PubMed: 23969093]

Glasser MF, & van Essen DC (2011). Mapping human cortical areas in vivo based on myelin content as revealed by T1- and T2-weighted MRI. Journal of Neuroscience, 31(32), 11597–11616. 10.1523/JNEUROSCI.2180-11.2011 [PubMed: 21832190]

Goldstein RZ, & Volkow ND (2002). Drug addiction and its underlying neurobiological basis: Neuroimaging evidence for the involvement of the frontal cortex. In American Journal of Psychiatry (Vol. 159, Issue 10, pp. 1642–1652). NIH Public Access. 10.1176/appi.ajp.159.10.1642 [PubMed: 12359667]

Goldstein RZ, & Volkow ND (2011). Dysfunction of the prefrontal cortex in addiction: Neuroimaging findings and clinical implications. In Nature Reviews Neuroscience (Vol. 12, Issue 11). 10.1038/nrn3119

Gossop M (1990). The development of a short opiate withdrawal scale (SOWS). Addictive Behaviors, 15(5). 10.1016/0306-4603(90)90036-W

Gossop M, Darke S, Griffiths P, Hando J, Powis B, Hall W, & Strang J (1995). The Severity of Dependence Scale (SDS): psychometric properties of the SDS in English and Australian samples of heroin, cocaine and amphetamine users. Addiction, 90(5), 607–614. 10.1046/j.1360-0443.1995.9056072.x [PubMed: 7795497]

Haber SN, Liu H, Seidlitz J, & Bullmore E (2022). Prefrontal connectomics: from anatomy to human imaging. In Neuropsychopharmacology (Vol. 47, Issue 1). 10.1038/s41386-021-01156-6

He Q, Li D, Turel O, Bechara A, & Hser YI (2020). White matter integrity alternations associated with cocaine dependence and long-term abstinence: Preliminary findings. Behavioural Brain Research, 379. 10.1016/j.bbr.2019.112388

Heatherton TF, Kozlowski LynnT., Frecker RC, & Fagerstrom K-O (1991). The Fagerström Test for Nicotine Dependence: a revision of the Fagerstrom Tolerance Questionnaire. British Journal of Addiction, 86(9), 1119–1127. 10.1111/j.1360-0443.1991.tb01879.x [PubMed: 1932883]

Heinz AJ, Epstein DH, Schroeder JR, Singleton EG, Heishman SJ, & Preston KL (2006). Heroin and cocaine craving and use during treatment: Measurement validation and potential relationships. Journal of Substance Abuse Treatment, 31(4). 10.1016/j.jsat.2006.05.009

Hikosaka O (2010). The habenula: From stress evasion to value-based decision-making. In Nature Reviews Neuroscience (Vol. 11, Issue 7). 10.1038/nrn2866

Iglesias JE, Insausti R, Lerma-Usabiaga G, Bocchetta M, van Leemput K, Greve DN, van der Kouwe A, Fischl B, Caballero-Gaudes C, & Paz-Alonso PM (2018). A probabilistic atlas of the human thalamic nuclei combining ex vivo MRI and histology. Neuroimage, 183, 314–326. 10.1016/j.neuroimage.2018.08.012 [PubMed: 30121337]

Jastak S, & Wilkinson G (1993). Wide Range Achievement Test—Revised 3. Wilmington, DE: Jastak Associates.

Jbabdi S, Sotiropoulos SN, Haber SN, van Essen DC, & Behrens TE (2015). Measuring macroscopic brain connections in vivo. In Nature Neuroscience (Vol. 18, Issue 11). 10.1038/nn.4134

Jeurissen B, Tournier JD, Dhollander T, Connelly A, & Sijbers J (2014). Multi-tissue constrained spherical deconvolution for improved analysis of multi-shell diffusion MRI data. NeuroImage, 103. 10.1016/j.neuroimage.2014.07.061

Jhou TC, Fields HL, Baxter MG, Saper CB, & Holland PC (2009). The Rostromedial Tegmental Nucleus (RMTg), a GABAergic Afferent to Midbrain Dopamine Neurons, Encodes Aversive Stimuli and Inhibits Motor Responses. Neuron, 61(5), 786–800. 10.1016/j.neuron.2009.02.001 [PubMed: 19285474]

Jhou TC, Good CH, Rowley CS, Xu S-P, Wang H, Burnham NW, Hoffman AF, Lupica CR, & Ikemoto S (2013). Cocaine drives aversive conditioning via delayed activation of dopamine-responsive habenular and midbrain pathways. Journal of Neuroscience, 33(17), 7501–7512. 10.1523/JNEUROSCI.3634-12.2013 [PubMed: 23616555]

Jordan CJ, & Andersen SL (2017). Sensitive periods of substance abuse: Early risk for the transition to dependence. In Developmental Cognitive Neuroscience (Vol. 25). 10.1016/j.dcn.2016.10.004

Kampman KM, Volpicelli JR, Mcginnis DE, Alterman AT, Weinrieb RM, D'Angelo L, & Epperson LE (1998). Reliability and validity of the cocaine selective severity assessment. Addictive Behaviors, 23(4), 449–461. 10.1016/S0306-4603(98)00011-2 [PubMed: 9698974]

Kaufman MJ, Levin JM, Ross MH, Lange N, Rose SL, Kukes TJ, Mendelson JH, Lukas SE, Cohen BM, & Renshaw PF (1998). Cocaine-induced cerebral vasoconstriction detected in humans with magnetic resonance angiography. Journal of the American Medical Association, 279(5). 10.1001/jama.279.5.376

Kim J, Naidich TP, Ely BA, Yacoub E, de Martino F, Fowkes ME, Goodman WK, & Xu J (2016). Human habenula segmentation using myelin content. NeuroImage, 130, 145–156. 10.1016/j.neuroimage.2016.01.048 [PubMed: 26826517]

Kim U, & Lee T (2012). Topography of descending projections from anterior insular and medial prefrontal regions to the lateral habenula of the epithalamus in the rat. European Journal of Neuroscience, 35(8), 1253–1269. 10.1111/j.1460-9568.2012.08030.x [PubMed: 22512256]

Koob GF, & Volkow ND (2016). Neurobiology of addiction: a neurocircuitry analysis. In The Lancet Psychiatry (Vol. 3, Issue 8, pp. 760–773). Elsevier Ltd. 10.1016/S2215-0366(16)00104-8 [PubMed: 27475769]

Li B, Piriz J, Mirrione M, Chung C, Proulx CD, Schulz D, Henn F, & Malinow R (2011). Synaptic potentiation onto habenula neurons in the learned helplessness model of depression. Nature, 470(7335). 10.1038/nature09742

Li W, Li Q, Zhu J, Qin Y, Zheng Y, Chang H, Zhang D, Wang H, Wang L, Wang Y, & Wang W (2013). White matter impairment in chronic heroin dependence: A quantitative DTI study. Brain Research, 1531. 10.1016/j.brainres.2013.07.036

Li W, Zhu J, Li Q, Ye J, Chen J, Liu J, Li Z, Li Y, Yan X, Wang Y, & Wang W (2016). Brain white matter integrity in heroin addicts during methadone maintenance treatment is related to relapse propensity. Brain and Behavior, 6(2). 10.1002/brb3.436

Liu H, Li L, Hao Y, Cao D, Xu L, Rohrbaugh R, Xue Z, Hao W, Shan B, & Liu Z (2008). Disrupted white matter integrity in heroin dependence: A controlled study utilizing diffusion tensor imaging. American Journal of Drug and Alcohol Abuse, 34(5). 10.1080/00952990802295238

Ma L, Steinberg JL, Wang Q, Schmitz JM, Boone EL, Narayana PA, & Moeller FG (2017). A preliminary longitudinal study of white matter alteration in cocaine use disorder subjects. Drug and Alcohol Dependence, 173. 10.1016/j.drugalcdep.2016.12.016

Mahler SV, & Aston-Jones GS (2012). Fos activation of selective afferents to ventral tegmental area during cue-induced reinstatement of cocaine seeking in rats. Journal of Neuroscience, 32(38), 13309–13325. 10.1523/JNEUROSCI.2277-12.2012 [PubMed: 22993446]

Martin JA, Caccamise A, Werner CT, Viswanathan R, Polanco JJ, Stewart AF, Thomas SA, Sim FJ, & Dietz DM (2018). A Novel Role for Oligodendrocyte Precursor Cells (OPCs) and Sox10 in Mediating Cellular and Behavioral Responses to Heroin. Neuropsychopharmacology, 43(6). 10.1038/npp.2017.303

Martin-Schild S, Albright KC, Hallevi H, Barreto AD, Philip M, Misra V, Grotta JC, & Savitz SI (2010). Intracerebral hemorrhage in cocaine users. Stroke, 41(4). 10.1161/STROKEAHA.109.573147

Mathis V, Barbelivien A, Majchrzak M, Mathis C, Cassel JC, & Lecourtier L (2017). The Lateral Habenula as a Relay of Cortical Information to Process Working Memory. Cerebral Cortex (New York, N.Y. : 1991), 27(12), 5485–5495. 10.1093/cercor/bhw316

Mathis V, & Kenny PJ (2019). From controlled to compulsive drug-taking: The role of the habenula in addiction. In Neuroscience and Biobehavioral Reviews (Vol. 106). 10.1016/j.neubiorev.2018.06.018

Mathis VP, Williams M, Fillinger C, & Kenny PJ (2021). Networks of habenula-projecting cortical neurons regulate cocaine seeking. Science Advances, 7(45). 10.1126/sciadv.abj2225

Matsumoto M, & Hikosaka O (2009). Representation of negative motivational value in the primate lateral habenula. Nature Neuroscience, 12(1), 77–84. 10.1038/nn.2233 [PubMed: 19043410]

McLellan AT, Kushner H, Metzger D, Peters R, Smith L, Grissom G, Pettinati H, & Argeriou M (1992). The fifth edition of the addiction severity index. Journal of Substance Abuse Treatment, 9(3), 199–213. 10.1016/0740-5472(92)90062-S [PubMed: 1334156]

Meye FJ, Soiza-Reilly M, Smit T, Diana MA, Schwarz MK, & Mameli M (2016). Shifted pallidal co-release of GABA and glutamate in habenula drives cocaine withdrawal and relapse. Nature Neuroscience, 19(8), 1019–1024. 10.1038/nn.4334 [PubMed: 27348214]

Meye FJ, Valentinova K, Lecca S, Marion-Poll L, Maroteaux MJ, Musardo S, Moutkine J, Gardoni F, Huganir RL, Georges F, & Mameli M (2015). Cocaine-evoked negative symptoms require AMPA receptor trafficking in the lateral habenula. Nature Neuroscience, 18(3), 376–380. 10.1038/nn.3923 [PubMed: 25643299]

Mizumori SJY, & Baker PM (2017). The Lateral Habenula and Adaptive Behaviors. In Trends in Neurosciences (Vol. 40, Issue 8). 10.1016/j.tins.2017.06.001

Montoya-Filardi A, & Mazón M (2017). The addicted brain: Imaging neurological complications of recreational drug abuse. Radiologia (English Edition), 59(1). 10.1016/j.rxeng.2016.12.003

Murty VP, Shermohammed M, Smith D. v., Carter RMK, Huettel SA, & Adcock RA (2014). Resting state networks distinguish human ventral tegmental area from substantia nigra. NeuroImage, 100. 10.1016/j.neuroimage.2014.06.047

Narayana PA, Herrera JJ, Bockhorst KH, Esparza-Coss E, Xia Y, Steinberg JL, & Moeller FG (2014). Chronic cocaine administration causes extensive white matter damage in brain: Diffusion tensor imaging and immunohistochemistry studies. Psychiatry Research - Neuroimaging, 221(3). 10.1016/j.pscychresns.2014.01.005

Navailles S, Guillem K, Vouillac-Mendoza C, & Ahmed SH (2015). Coordinated recruitment of cortical-subcortical circuits and ascending dopamine and serotonin neurons during inhibitory control of cocaine seeking in rats. Cerebral Cortex, 25(9), 3167–3181. 10.1093/cercor/bhu112 [PubMed: 24872521]

Pimentel E, Sivalingam K, Doke M, & Samikkannu T (2020). Effects of Drugs of Abuse on the Blood-Brain Barrier: A Brief Overview. In Frontiers in Neuroscience (Vol. 14). 10.3389/fnins.2020.00513

Preuss TM, & Goldman-Rakic PS (1987). Crossed corticothalamic and thalamocortical connections of macaque prefrontal cortex. Journal of Comparative Neurology, 257(2), 269–281. 10.1002/cne.902570211 [PubMed: 3571529]

Pribiag H, Shin S, Wang EH-J, Sun F, Datta P, Okamoto A, Guss H, Jain A, Wang X-Y, de Freitas B, Honma P, Pate S, Lilascharoen V, Li Y, & Lim BK (2021). Ventral pallidum DRD3 potentiates a pallido-habenular circuit driving accumbal dopamine release and cocaine seeking. Neuron. 10.1016/j.neuron.2021.05.002

R Core Team. (n.d.). R: A Language and Environment for Statistical Computing. In R Foundation for Statistical Computing. R Foundation for Statistical Computing.

Ritchie SJ, Cox SR, Shen X, Lombardo M. v., Reus LM, Alloza C, Harris MA, Alderson HL, Hunter S, Neilson E, Liewald DCM, Auyeung B, Whalley HC, Lawrie SM, Gale CR, Bastin ME, McIntosh AM, & Deary IJ (2018). Sex differences in the adult human brain: Evidence from 5216 UK biobank participants. Cerebral Cortex, 28(8). 10.1093/cercor/bhy109

Roddy DW, Roman E, Rooney S, Andrews S, Farrell C, Doolin K, Levins KJ, Tozzi L, Tierney P, Barry D, Frodl T, O'Keane V, & O'Hanlon E (2018). Awakening neuropsychiatric research into the stria medullaris: Development of a diffusion-weighted imaging tractography protocol of this key limbic structure. Frontiers in Neuroanatomy, 12. 10.3389/fnana.2018.00039

Romero MJ, Asensio S, Palau C, Sanchez A, & Romero FJ (2010). Cocaine addiction: Diffusion tensor imaging study of the inferior frontal and anterior cingulate white matter. Psychiatry Research - Neuroimaging, 181(1). 10.1016/j.pscychresns.2009.07.004

Safadi Z, Grisot G, Jbabdi S, Behrens TE, Heilbronner SR, McLaughlin NCR, Mandeville J, Versace A, Phillips ML, Lehman JF, Yendiki A, & Haber SN (2018). Functional segmentation of the anterior limb of the internal capsule: Linking white matter abnormalities to specific connections. Journal of Neuroscience, 38(8). 10.1523/JNEUROSCI.2335-17.2017

Savjani RR, Velasquez KM, Thompson-Lake DGY, Baldwin PR, Eagleman DM, de La Garza R, & Salas R (2014). Characterizing white matter changes in cigarette smokers via diffusion tensor imaging. Drug and Alcohol Dependence, 145. 10.1016/j.drugalcdep.2014.10.006

Sheehan D. v., Lecrubier Y, Sheehan KH, Amorim P, Janavs J, Weiller E, Hergueta T, Baker R, & Dunbar GC (1998). The Mini-International Neuropsychiatric Interview (M.I.N.I.): The development and validation of a structured diagnostic psychiatric interview for DSM-IV and ICD-10. Journal of Clinical Psychiatry, 59(SUPPL. 20).

Shelton L, Pendse G, Maleki N, Moulton EA, Lebel A, Becerra L, & Borsook D (2012). Mapping pain activation and connectivity of the human habenula. Journal of Neurophysiology, 107(10). 10.1152/jn.00012.2012

Smith RE, Tournier JD, Calamante F, & Connelly A (2012). Anatomically-constrained tractography: Improved diffusion MRI streamlines tractography through effective use of anatomical information. NeuroImage, 62(3), 1924–1938. 10.1016/j.neuroimage.2012.06.005 [PubMed: 22705374]

Smith SM, Jenkinson M, Woolrich MW, Beckmann CF, Behrens TEJ, Johansen-Berg H, Bannister PR, de Luca M, Drobnjak I, Flitney DE, Niazy RK, Saunders J, Vickers J, Zhang Y, de Stefano N, Brady JM, & Matthews PM (2004). Advances in functional and structural MR image analysis and implementation as FSL. NeuroImage, 23(SUPPL. 1). 10.1016/j.neuroimage.2004.07.051

Squeglia LM, Jacobus J, & Tapert SF (2009). The influence of substance use on adolescent brain development. Clinical EEG and Neuroscience, 40(1). 10.1177/155005940904000110

Stephenson-Jones M, Floros O, Robertson B, & Grillner S (2012). Evolutionary conservation of the habenular nuclei and their circuitry controlling the dopamine and 5-hydroxytryptophan (5-HT) systems. Proceedings of the National Academy of Sciences of the United States of America, 109(3). 10.1073/pnas.1119348109

Strotmann B, Heidemann RM, Anwander A, Weiss M, Trampel R, Villringer A, & Turner R (2014). High-resolution MRI and diffusion-weighted imaging of the human habenula at 7 Tesla. Journal of Magnetic Resonance Imaging, 39(4), 1018–1026. 10.1002/jmri.24252 [PubMed: 24259421]

Sutherland RJ (1982). The dorsal diencephalic conduction system: A review of the anatomy and functions of the habenular complex. Neuroscience and Biobehavioral Reviews, 6(1). 10.1016/0149-7634(82)90003-3

Tian X, Ru Q, Xiong Q, Yue K, Chen L, Ma B, Gan W, Si Y, Xiao H, & Li C (2017). Neurotoxicity induced by methamphetamine-heroin combination in PC12 cells. Neuroscience Letters, 647. 10.1016/j.neulet.2017.03.005

Tiffany ST, Singleton E, Haertzen CA, & Henningfield JE (1993). The development of a cocaine craving questionnaire. Drug and Alcohol Dependence, 34(1), 19–28. 10.1016/0376-8716(93)90042-0 [PubMed: 8174499]

Tisdall L, MacNiven KH, Padula CB, Leong JK, & Knutson B (2022). Brain tract structure predicts relapse to stimulant drug use. PNAS, 119(26). https://www.pnas.org/doi/abs/10.1073/pnas.2116703119

Tondo LP, Viola TW, Fries GR, Kluwe-Schiavon B, Rothmann LM, Cupertino R, Ferreira P, Franco AR, Lane SD, Stertz L, Zhao Z, Hu R, Meyer T, Schmitz JM, Walss-Bass C, & Grassi-Oliveira R (2021). White matter deficits in cocaine use disorder: convergent evidence from in vivo diffusion tensor imaging and ex vivo proteomic analysis. Translational Psychiatry, 11(1). 10.1038/s41398-021-01367-x

Tournier JD, Calamante F, & Connelly A (2007). Robust determination of the fibre orientation distribution in diffusion MRI: Non-negativity constrained super-resolved spherical deconvolution. NeuroImage, 35(4), 1459–1472. 10.1016/j.neuroimage.2007.02.016 [PubMed: 17379540]

Tournier JD, Calamante F, & Connelly A (2009). Improved probabilistic streamlines tractography by 2 nd order integration over fibre orientation distributions.

Tustison NJ, Avants BB, Cook PA, Zheng Y, Egan A, Yushkevich PA, & Gee JC (2010). N4ITK: Improved N3 bias correction. IEEE Transactions on Medical Imaging, 29(6), 1310–1320. 10.1109/TMI.2010.2046908 [PubMed: 20378467]

Vadovičová K (2014). Affective and cognitive prefrontal cortex projections to the lateral habenula in humans. Frontiers in Human Neuroscience, 8(October). 10.3389/fnhum.2014.00819

Vaquero L, Cámara E, Sampedro F, Pérez de los Cobos J, Batlle F, Fabregas JM, Sales JA, Cervantes M, Ferrer X, Lazcano G, Rodríguez-Fornells A, & Riba J (2017). Cocaine addiction is associated with abnormal prefrontal function, increased striatal connectivity and sensitivity to monetary incentives, and decreased connectivity outside the human reward circuit. Addiction Biology, 22(3). 10.1111/adb.12356

Velasquez KM, Molfese DL, & Salas R (2014). The role of the habenula in drug addiction. In Frontiers in Human Neuroscience (Vol. 8, Issue MAR). Frontiers Media S. A. 10.3389/fnhum.2014.00174

Wang X, Yu R, Zhou X, Liao Y, Tang J, Liu T, Shan B, & Hao W (2013). Reversible brain white matter microstructure changes in heroin addicts: A longitudinal study. Addiction Biology, 18(4). 10.1111/j.1369-1600.2011.00316.x

Wechsler D (1999). Manual for the Wechsler abbreviated intelligence scale (WASI). In WASI.

Wollman SC, Alhassoon OM, Stern MJ, Hall MG, Rompogren J, Kimmel CL, & Perez-Figueroa AM (2015). White matter abnormalities in long-term heroin users: A preliminary neuroimaging meta-analysis. American Journal of Drug and Alcohol Abuse, 41(2). 10.3109/00952990.2014.985829

Woolrich MW, Jbabdi S, Patenaude B, Chappell M, Makni S, Behrens T, Beckmann C, Jenkinson M, & Smith SM (2009). Bayesian analysis of neuroimaging data in FSL. NeuroImage, 45(1 Suppl). 10.1016/j.neuroimage.2008.10.055

Ye L, Allen WE, Thompson KR, Tian Q, Hsueh B, Ramakrishnan C, Wang AC, Jennings JH, Adhikari A, Halpern CH, Witten IB, Barth AL, Luo L, McNab JA, & Deisseroth K (2016). Wiring and Molecular Features of Prefrontal Ensembles Representing Distinct Experiences. Cell, 165(7). 10.1016/j.cell.2016.05.010

Yendiki A, Aggarwal M, Axer M, Howard AFD, van Walsum AM van C, & Haber SN (2022). Post mortem mapping of connectional anatomy for the validation of diffusion MRI. NeuroImage, 256. 10.1016/j.neuroimage.2022.119146

Zahm DS, & Root DH (2017). Review of the cytology and connections of the lateral habenula, an avatar of adaptive behaving. In Pharmacology Biochemistry and Behavior (Vol. 162, pp. 3–21). Elsevier Inc. 10.1016/j.pbb.2017.06.004 [PubMed: 28647565]

Highlights:

- Diffusion MRI tractography models a plausible PFC-Hb connection in human brain
- People with cocaine addiction showed reduced PFC-Hb microstructural coherence
- Results showed a similar pattern in heroin addiction, extending preclinical models
- Impairments were associated with earlier onset of drug use in the addiction groups

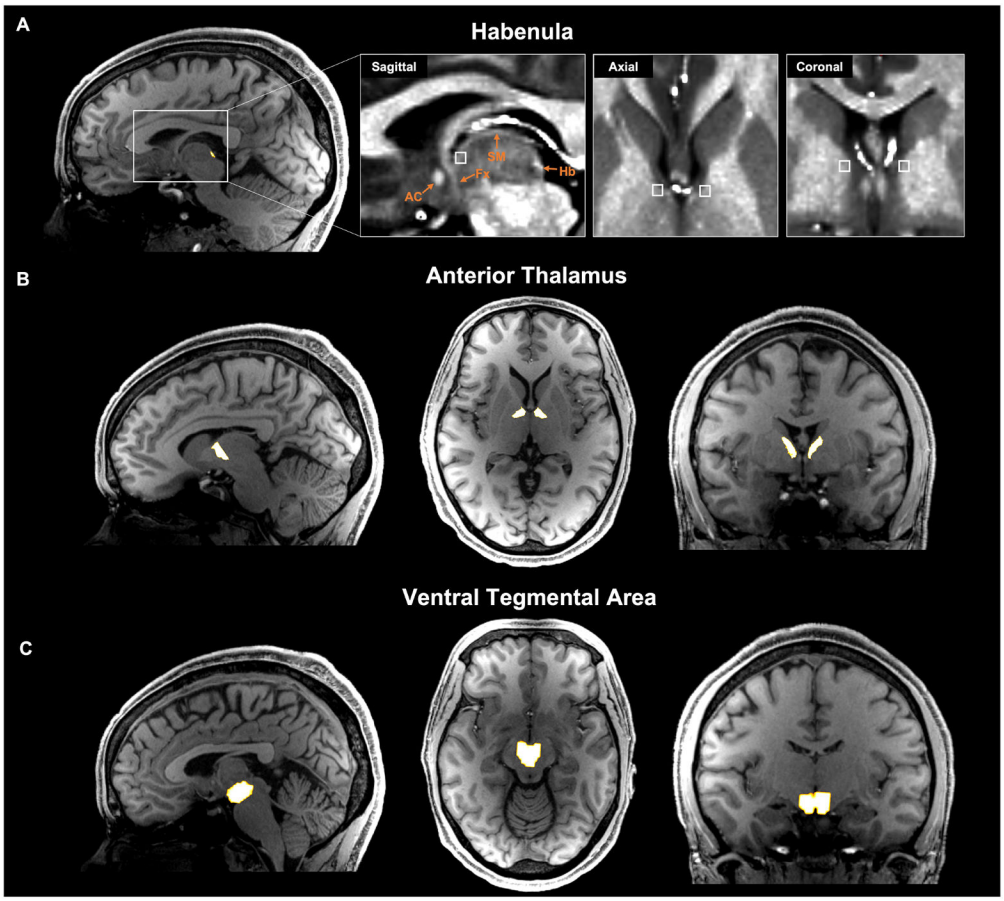

Figure 1.

Subcortical seed region and inclusion mask selection for tractography analysis from one representative subject. (A) Habenula segmentation mask overlaid on T1w image. Anatomical landmarks are identified in the expanded boxed region with T1w/T2w image. Streamlines were constrained to pass through an individually defined anterior stria medullaris (white box) mask. AC=anterior commissure; Fx=fornix; Hb=habenula; SM=stria medullaris. (B) Anterior thalamus mask generated using Freesurfer's anteroventral and ventral anterior nuclei segmentations. (C) Ventral tegmental area mask derived from an atlas of the midbrain in MNI space and warped to individual space.

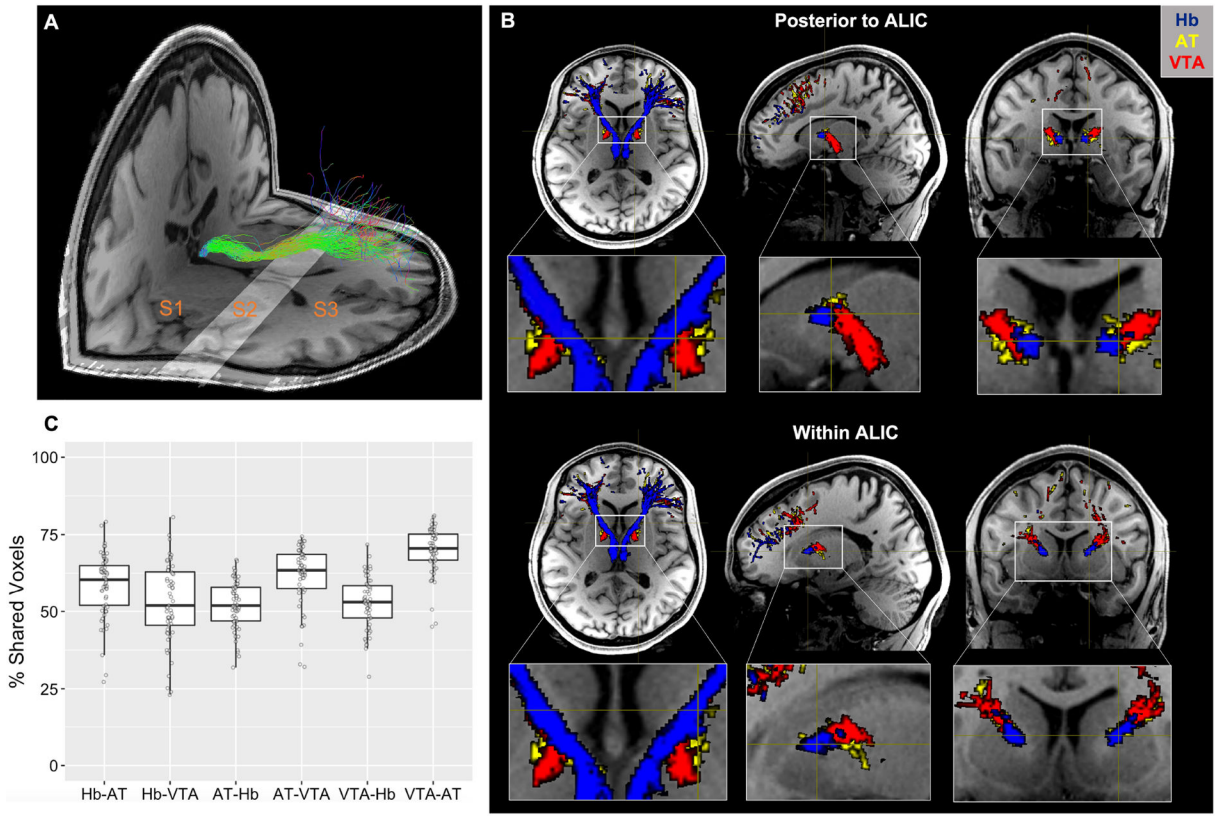

Figure 2.

Habenula tract and its topological feature with the control tracts within and posterior to the anterior limb of the internal capsule (ALIC) in one representative subject. (A) Designation of subsections using anatomical landmarks with habenula tracts (green) overlaid: S1, anterior of the habenula to anterior thalamus; S2, anterior of the thalamus to anterior caudate; S3, anterior of the caudate to PFC grey matter. (B) Topology of the habenula tracts (blue) immediately posterior to (upper panel) and within (lower panel) the ALIC (S2) compared to control AT (yellow) and VTA (red) tracts. The habenula tracts display a ventral-medial trajectory relative to the control tracts that is maintained throughout the ALIC. (C) Percentage of voxels shared between masks of each tract in CUD subjects and their matched CTL group within S2 (e.g., Hb-AT denotes the percentage of Hb tract voxels that are also contained within the AT tract, see main text for detail). Boxplot represents the median (center line), interquartile range (box), and 1.5x the interquartile range (whiskers).

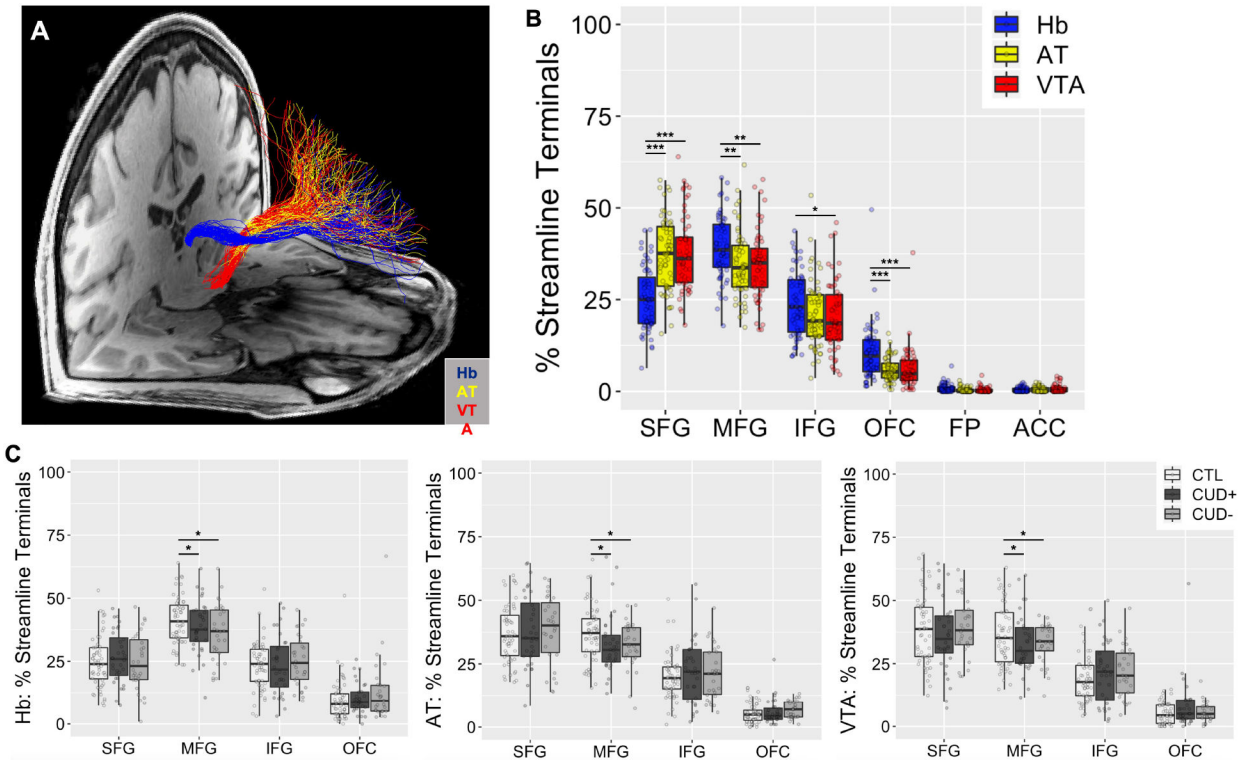

Figure 3.

Distinct PFC-Hb streamline terminal distributions as compared to those from control seed regions. (A) Tracts seeded in subcortical seeds, the habenula (Hb, blue), anterior thalamus (AT, yellow), and ventral tegmental area (VTA, red), with streamline terminals in the PFC from a representative subject. (B) Comparison of the distribution of streamline terminals in the PFC for tracts seeded in subcortical seeds, averaged between left and right sides. (C) CUD vs. CTL group comparisons of the distribution of streamline terminals from each of the subcortical seeds. *p < .05, **p < .01, ***p < .001. SFG = superior frontal gyrus; MFG = middle frontal gyrus; IFG = inferior frontal gyrus; OFC = orbitofrontal cortex; FP = frontal pole; ACC = anterior cingulate cortex; CTL = control individuals; CUD+ = currently using cocaine-addicted individuals; CUD− = short-term abstinent cocaine-addicted individuals. Boxplots represent the median (center line), interquartile range (box), and 1.5x the interquartile range (whiskers).

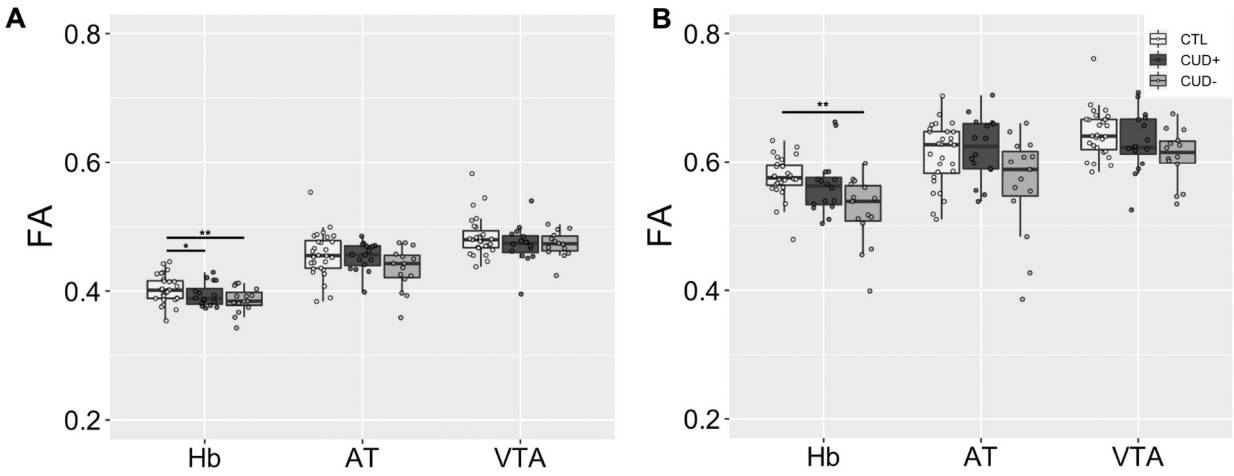

Figure 4.

Group comparisons of FA averaged across the entire tract (A) and within the ALIC subsection (B). *p < .05, **p < .01, ***p < .001. FA = fractional anisotropy; Hb = habenula; AT = anterior thalamus; VTA = ventral tegmental area; CTL = control individuals; CUD+ = currently using cocaine-addicted individuals; CUD− = short-term abstinent cocaine-addicted individuals. Boxplots represent the median (center line), interquartile range (box), and 1.5x the interquartile range (whiskers).

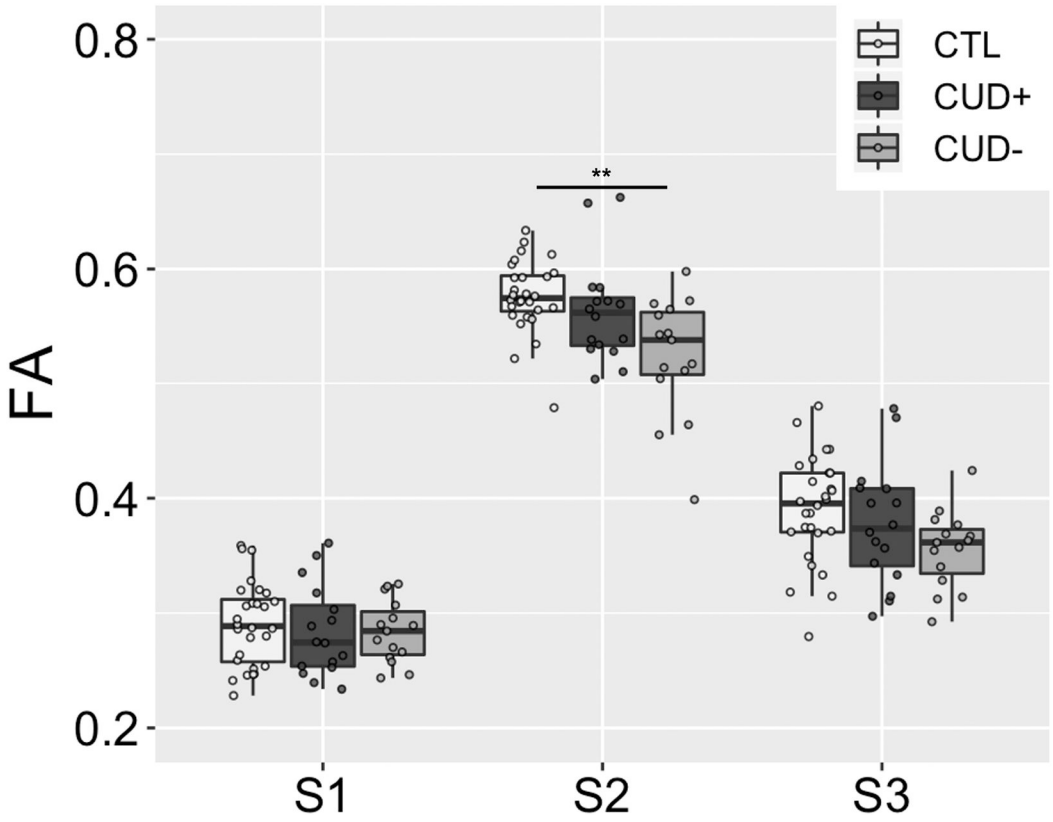

Figure 5.

Group comparison of FA in subsections S1, S2, and S3 of the PFC-Hb tract. FA = fractional anisotropy; CTL = control individuals; CUD+ = currently using cocaine-addicted individuals; CUD− = short-term abstinent cocaine-addicted individuals. Boxplot represents the median (center line), interquartile range (box), and 1.5x the interquartile range (whiskers). Note that S2 in this figure and Figure 4B Hb show the same data.

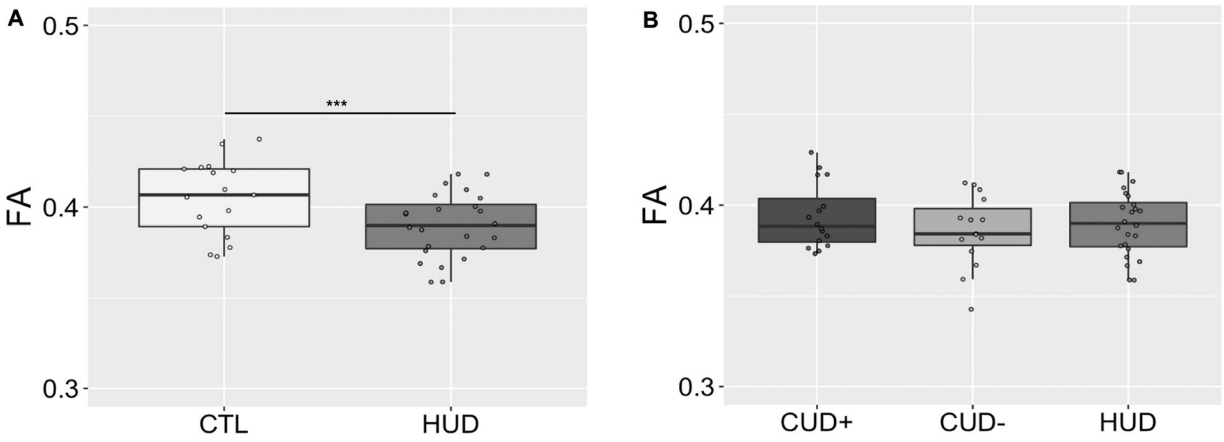

Figure 6.

Group comparisons of FA averaged across the entire prefrontal cortex-habenula tract in the heroin addiction group compared with healthy controls (A) and cocaine addiction groups (B). *p < .05, **p < .01, ***p < .001. FA = fractional anisotropy; HUD = heroin-addicted individuals CTL = control individuals; CUD+ = currently using cocaine-addicted individuals; CUD− = short-term abstinent cocaine-addicted individuals. Boxplots represent the median (center line), interquartile range (box), and 1.5x the interquartile range (whiskers).

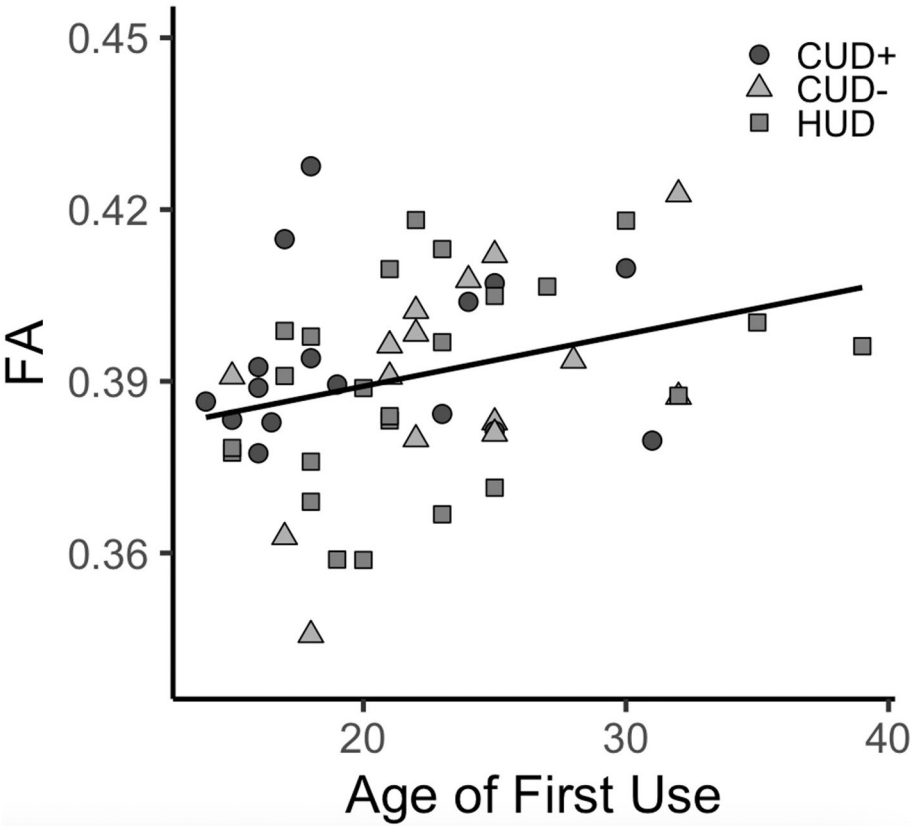

Figure 7.

Correlation of FA averaged across the entire prefrontal cortex-habenula tract with age of first cocaine (CUD+/CUD−) or heroin (HUD) use ($r = 0.30$, $p = .025$).

Table 1

Demographic, psychometric, and substance use characteristics of study participants

	CTL N = 28	CUD+ N = 16	CUD− N=15	CTL N = 17	HUD N = 24	Test Statistic CTL/CUD+/CUD−	CTL/HUD	CUD+/CUD−/HUD
Demographics								
Age	41.7 ± 7.5	46.8 ± 7.5	45.5 ± 9.4	40.1 ± 10.3	39.9 ± 9.4	F = 1.86	U = 218.0	H = 6.97
Sex (female/male)	10/18	4/12	4/11	7/10	6/18	χ^2 = 1.23	χ^2 = 0.57	χ^2 = 0.02
Race (Black/White/Other/no response)	22/2/2/2	14/0/1/1[d]	8/4/2/1[d]	4/9/4/0	1/18/2/3[b,c]	χ^2 = 7.80	χ^2 = 7.90	χ^2 = 32.0*
Ethnicity (Hispanic/Non-Hispanic/no response)	4/23/1	2/12/2[d]	3/1l/1[d]	3/13/1	9/15/0[b,c]	χ^2 = 1.64	χ^2 = 3.04	χ^2 = 56.0*
Education (years)	14.3 ± 2.1[b,c]	12.4 ± 2.1[a]	11.9 ± 2.0[a]	17.6 ± 3.6	11.7 ± 1.7	F = 8.67*	U = 417.5*	F = 0.61
Psychometrics								
WRAT-3 Reading Scaled Score	100.8 ± 10.8[b]	89.6 ± 11.9[a]	95.9 ± 13.3	110.3 ± 6.8	92.5 ± 12.0	H = 8.72*	t = 6.03*	F = 1.11
WASI Matrix Reasoning Scaled Score	10.6 ± 2.8[b]	8.3 ± 3.4[a,c]	11.1 ± 2.8[b]	12.2 ± 3.1	9.7 ± 3.2	H = 7.75*	t = 2.49	F = 2.94
Beck Depression Inventory	2.3 ± 3.0[b,c]	7.3 ± 7.0[a]	8.1 ± 8.4[a]	3.2 ± 4.3	16.0 ± 13.3	H = 12.20*	U = 56.0*	H = 5.48
Substance use								
Past 30-day alcohol use (# of days)	1.2 ± 3.9[b]	4.8 ± 3.2[a,c,d]	1.0 ± 3.5[b]	4.2 ± 9.1	0.1 ± 0.2[b]	H = 10.85*	U = 255.0*	H = 22.00*
Cigarette use (current/past/never)	2/6/20[b,c]	15/1/0[a]	11/3/1[a]	0/2/15	24/0/0	χ^2 = 38.69*	χ^2 = 41.00*	χ^2 = 8.52
Fagerström Test for Nicotine Dependence	0.8 ± 1.6[c]	1.5 ± 2.4[d]	2.9 ± 2.2[a]	0.0 ± 0.0	3.8 ± 1.3[b]	H = 11.07*	U = 0*	H = 9.00*
Age of first DOC use (years)	---	20.2 ± 5.4	23.3 ± 4.9	---	22.6 ± 6.2	---	---	F = 1.34
Duration of regular DOC use (years)	---	23.4 ± 10.0	16.5 ± 8.7	---	13.0 ± 7.8	---	---	H = 9.69
Duration of current DOC abstinence (days)	---	3.3 ± 3.5[c,d]	89.2 ± 62.1[b]	---	136.6 ± 190.0[b]	---	---	H = 28.45*
Past 30-day DOC use (# of days)	---	13.4 ± 8.4[c,d]	3.4 ± 7.0[b]	---	0.46 ± 1.4[b]	---	---	H = 32.14*
Withdrawal (adjusted score)	---	21.8 ± 4.1	16.3 ± 12.5	---	14.7 ± 15.1	---	---	H = 3.03
Craving (adjusted score)	---	21.6 ± 13.1[c]	8.3 ± 11.5[b,d]	---	18.8 ± 7.2[c]	---	---	H = 13.77*
Severity of Dependence Scale	---	4.3 ± 3.6[c,d]	8.2 ± 5.8[b]	---	11.0 ± 3.2[b]	---	---	H = 16.81*

χ^2 tests were used for categorical variables; ANOVA or Student's t-test for normally distributed continuous variables; and Kruskal-Wallis H or Mann-Whitney U for non-normally distributed continuous variables. Data are expressed as frequencies or mean ± standard deviation.

Note: For eight of the variables, up to three participants in each group had missing data.

[*] Significant at $p < .05$, corrected for multiple comparisons

[a] Significant difference from CTL

[b] Significant difference from CUD+

[c] Significant difference from CUD−

[d] Significant difference from HUD

Key resources table

REAGENT or RESOURCE	SOURCE	IDENTIFIER
Antibodies		
Bacterial and virus strains		
Biological samples		
Chemicals, peptides, and recombinant proteins		
Critical commercial assays		
Deposited data		
Experimental models: Cell lines		

REAGENT or RESOURCE	SOURCE	IDENTIFIER
Experimental models: Organisms/strains		
Oligonucleotides		
Recombinant DNA		
Software and algorithms		
MRtrix3	Smith et al., 2004	https://www.mrtrix.org/
FSL dtifit	Woolrich et al., 2009	https://fsl.fmrib.ox.ac.uk/fsl/fslwiki/
Freesurfer recon-all	Fischl et al., 2002	https://surfer.nmr.mgh.harvard.edu/
Habenula segmentation	Kim et al., 2016	https://github.com/junqianxulab/habenula_segmentation
Habenula resampling and shape optimization	Ely et al., 2019	https://github.com/junqianxulab/Habenula_fMRI_ROIs
VTA segmentation	Murty et al., 2014	https://www.adcocklab.org/neuroimaging-tools
Other		